Published by :
http://www.ijert.org

International Journal of Engineering Research & Technology (IJERT)
ISSN: 2278-0181
Vol. 14 Issue 06, June - 2025

Optimizing the Efficiency of Agricultural Direct Solar Dryers using Computational Fluid Dynamics

A Comparative CFD Analysis of Trapezoidal, Rectangular, and Triangular Dryer Design

Sarah Kobusingye; Twaibu Ssemwogerere; Asaph Keikara Muhumuza; Rebecca Muhumuza Nalule*
Busitema University, Tororo. Uganda.

***Abstract*—countries where traditional open sun drying is still widely used despite its limitations, including contamination risks and inefficiencies. This study explores the optimization of agricultural direct solar dryers using Computational Fluid Dynamics (CFD) to enhance drying efficiency, reduce food loss, and support sustainable agricultural practices. Using COMSOL Multiphysics, CFD simulations were conducted on three geometric designs of trapezium, rectangular, and triangular prism top-shaped dryers, to evaluate airflow patterns and temperature distribution over time. The analysis revealed that triangular prism geometries achieved superior airflow uniformity and temperature consistency, resulting in more effective drying performance. Airflow and heat distribution were analyzed at intervals of 0s, *45s*, *67.5s*, and 90s to capture transient behavior and evaluate steady-state performance. The triangular design minimized stagnation zones and supported optimal convective heat transfer throughout the chamber. These findings demonstrate the potential of CFD as a powerful tool in guiding the design and performance enhancement of solar dryers. By improving heat distribution and airflow dynamics, the optimized design reduces drying time, contamination risks, and post- harvest losses. The research supports the broader goals of food security and climate resilience by promoting energy-efficient, low-cost drying technologies suited for rural agricultural communities. Future work may include experimental validation and economic feasibility analysis to facilitate real-world application and adoption.**

***Keywords*—Solar drying, Computational Fluid Dynamics, Agricultural dryers, COMSOL Multiphysics, Sustainable agriculture**

INTRODUCTION

Agriculture plays a pivotal role in ensuring global food security and economic stability especially in developing regions where it constitutes a substantial share of Gross Domestic Product (GDP) and employment [1, 2]. However, the sector faces persistent challenges, one of the most critical being post-harvest losses. These losses account for up to 30–40% of food production in sub-Saharan Africa, largely due to inefficient drying, storage, and transportation systems [5, 6]. According to the Food and Agriculture Organization [1, 3], nearly one-third of all food produced globally is either lost or wasted, with a significant share occurring during post-harvest stages.

Drying is a key post-harvest operation that preserves agricultural products by reducing moisture content, thus extending shelf life and minimizing microbial spoilage. Traditional open sun drying is the most common method in rural settings due to its simplicity and low cost [4, 7]. However, it poses significant drawbacks including contamination by dust and insects, dependency on weather conditions, uneven drying, and significant quality deterioration [8, 9]. Consequently, there is growing demand for improved, hygienic, and energy-efficient alternatives.

Solar drying technologies provide a promising solution by harnessing renewable solar energy for food preservation. Direct solar dryers, in particular, offer the advantage of exposing products to solar radiation within a controlled enclosure, thus improving drying rates and protecting the product from contamination [10]. These systems not only enhance food quality and storage life but also contribute to climate resilience by reducing reliance on fossil fuels for thermal energy [11]. However, to ensure their effectiveness, solar dryers must be designed to maximize heat transfer and airflow uniformity throughout the drying chamber.

Computational Fluid Dynamics (CFD) offers a cost-effective, simulation-based approach for optimizing the design and operational efficiency of solar dryers. By solving the Navier-Stokes and energy equations numerically, CFD can model airflow, heat distribution, and moisture removal in complex geometries [12]. Previous studies have used CFD to enhance thermal uniformity and airflow patterns in dryers, reducing hot-spots and improving drying uniformity [13]. This study applies CFD simulations to evaluate the performance of three direct solar dryer geometries of trapezium, rectangular, and triangular prism top-shaped designs using COMSOL Multiphysics. The goal is to identify a geometry that optimizes airflow and heat distribution, thereby reducing drying time and post-harvest losses, while promoting energy-efficient and sustainable agricultural practices

II DRYER CONFIGURATIONS AND GEOMETRIC DESIGN

Three different geometric configurations of direct solar dryers were considered: rectangular, trapezoidal, and triangular prism top-shaped dryers. These designs were selected based on their relevance in agricultural communities and prior studies emphasizing structural simplicity and thermal efficiency. The internal drying chambers were dimensioned to have comparable volumes to ensure fair comparisons across geometries.

The geometries were modeled using SpaceClaim (ANSYS Inc.), a CAD tool that supports detailed geometric parameterization. Each model included the air inlet, drying chamber, and outlet vents, mimicking typical direct solar dryer structures used in rural communities.

III SIMULATION ENVIROMENT AND SOFTWARE

Simulations were carried out using COMSOL Multiphysics 5.6, a finite element analysis software well-suited for solving coupled partial differential equations involving fluid dynamics and heat transfer. The Laminar flow and Heat transfer in fluids physics modules were employed, assuming compressible air and steady solar heating during day light hours.

IV GOVERNING EQUATIONS

The simulations solved the coupled Navier-Stokes equations and energy conservation equation for airflow and temperature distribution:

Continuity equation (mass conservation):

$$\nabla \cdot \vec{v} = 0 \tag{1}$$

Navier-Stokes momentum equations:

$$\frac{\partial(\rho\vec{v})}{\partial t} + \nabla \cdot (\rho\vec{v}\vec{v}) = -\nabla p + \nabla \cdot \tau + \rho\vec{g} + \vec{F} \tag{2}$$

Energy Equations

$$\rho C_p \left(\frac{\partial T}{\partial t} + \vec{v} \cdot \nabla T \right) = k\nabla^2 T + S_h \tag{3}$$

The parameters used in these equations are as follows: $\vec{v}$ is the velocity vector of air in meters per second (m/s), T is the air temperature in Kelvin (K), $\vec{g}$ is the acceleration due to gravity, p is the pressure in Pascals (Pa), μ is the dynamic viscosity in Newton-seconds per square meter (Ns/m^2), and ρ is the air density in kilograms per cubic meter (kg/m^3). The shear stress tensor τ is defined by:

$$\tau = \mu \left(\nabla\vec{v} + (\nabla\vec{v})^T \right) - \frac{2}{3}\mu(\nabla \cdot \vec{v})I \tag{4}$$

where I is the unit tensor. Since the flow is incompressible, this simplifies to $\tau = \mu\nabla\vec{v}$.

Assuming the volume force vector $\vec{F}$ is zero, Equation (2) reduces to:

$$\frac{\partial(\rho\vec{v})}{\partial t} + \nabla \cdot (\rho\vec{v}\vec{v}) = -\nabla p + \nabla \cdot \tau + \rho\vec{g} \tag{5}$$

Assuming a constant thermal conductivity k, the energy equation further reduces to:

$$\frac{\partial T}{\partial t} + \vec{v} \cdot \nabla T = \alpha\nabla^2 T + S_h' \tag{6}$$

Where $\alpha = \frac{k}{\rho C_p}$ is the thermal diffusivity and $S'_h = \frac{S_h}{\rho C_p}$ is the normalized heat source term.

Figures 1(a) and 1(b) gives the geometry and mesh of the three different shapes respectively.

V BOUNDARY CONDITIONS

Appropriate boundary conditions were applied to each solar dryer model to simulate realistic operational environments. The inlet velocity was set at 0.5m/s to represent natural convection or mild forced flow, with an inlet air temperature of 293.15K.At the outlet, a pressure boundary condition was imposed with a gauge pressure of 0 Pa. The side walls of the dryers were modeled as adiabatic, implying no heat transfer through these surfaces. Transparent glass surfaces received a uniform solar heat flux of 1000 W/m2, representing steady solar irradiation during daylight. The ambient air pressure was fixed at 101325 Pa, and the simulation was run as a transient case up to 90 seconds with a time step of 0.5 seconds. A no-slip condition was enforced at all walls, ensuring the airflow velocity was zero at solid boundaries. Air properties were assumed to remain constant and dry throughout the simulation, and buoyancy effects were incorporated using the Boussinesq approximation to account for temperature-dependent density variations.

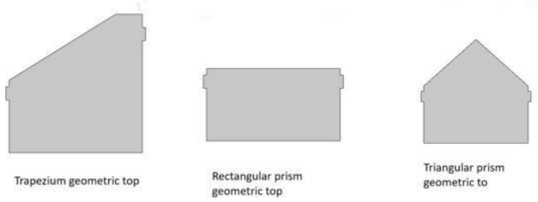

Figure(1a)Geometry of trapezium, rectangular and triangular top shaped designs respectively

Figure 1(b): M esh of trapezium, rectangular and triangular top shaped designs respectively

VI MESHING AND COVERGENCE.

Each geometry (Figure 1(a)) was discretized using unstructured tetrahedral meshes (Figure 1(b)) with refinement around the inlet and outlet. A mesh independence study confirmed result stability beyond a threshold element size. The relative tolerance for velocity and temperature convergence was set to 10^{-6}.

Simulations were executed on a workstation with Intel i7 CPU and 32 GB RAM velocity and temperature convergence was set to 10^{-6}.

VII PERFORMANCE METRICS

Dryer performance was evaluated based on several key parameters to understand and compare the effectiveness of different geometric designs. These parameters included the temperature distribution over time, velocity and airflow uniformity, and the presence of thermal gradients that highlight hot and cold zones. The presence of stagnation zones, where airflow is minimal, was also assessed, as these can hinder uniform drying. Additionally, the time taken to reach thermal steady-state was use to reach thermal steady-state was used as an indicator of the systems efficiency. Visualization tools such as contour and vector plots were employed to illustrate the thermal and fluid dynamics performance across the various dryer configurations

VIII AIRFLOW ANALYSIS OF THE TRAPEZIUM DESIGN

Figure 2 presents the temporal evolution of airflow within the first solar dryer design, analyzed at discrete time intervals: 0, 45, 67.5, and 90 seconds. These snapshots illustrate the dynamic changes in airflow patterns resulting from progressive thermal interactions within the drying chamber.

At the initial time (0 seconds, Figure 2a), airflow behavior is predominantly governed by the imposed boundary conditions. The velocity field remains relatively uniform, reflecting the absence of significant thermal gradients or internal convective forces. This condition represents the baseline state of the system prior to the onset of active thermal transport.

By 45 seconds (Figure 2b), thermal gradients begin to influence airflow, driven by solar heating of the chamber surfaces. Distinct changes in velocity magnitude and direction emerge, indicating the initiation of natural convective circulation within the dryer.

At 67.5 seconds (Figure 2c), the airflow patterns exhibit more developed and structured circulation zones. The interaction between heated internal surfaces and cooler incoming air enhances buoyancy-driven flows. These patterns reveal the geometry's influence on airflow channeling, particularly identifying zones of acceleration and potential stagnation.

By 90 seconds (Figure 2d), the system approaches a quasi-steady state. The airflow stabilizes, exhibiting coherent circulatory motion with reduced fluctuations. This mature flow regime is critical for uniform drying, as it facilitates consistent convective heat transfer and minimizes the occurrence of thermal dead zones.

Overall, the temporal airflow analysis provides insight into how the design geometry supports or restricts convective mechanisms essential for efficient thermal distribution. Effective airflow circulation ensures improved drying performance and reduced spatial temperature disparities within the dryer.

IX TEMPERATURE DISTRIBUTION ANALYSIS OF CASE 1

Figure 3 illustrates the evolution of temperature distribution within the solar dryer at four selected time intervals: 0, 45, 67.5, and 90 seconds. These temporal snapshots provide a comprehensive view of how heat propagates through the drying chamber as a result of solar exposure and convective transport.

At t = 0 s (Figure 3a), the temperature field is essentially uniform, representing the initial thermal state of the dryer. This baseline is crucial for assessing the subsequent temperature rise induced by solar heating and airflow dynamics.

By t = 45 s (Figure 3b), noticeable temperature gradients emerge within the dryer. Solar energy absorbed by the transparent surfaces begins to transfer into the air volume, resulting in an upward shift in internal temperature and the initiation of thermal stratification.

At t = 67.5 s (Figure 3c), the temperature field becomes more spatially differentiated, re- flecting the progression of internal heating. Stronger gradients appear along the walls and central axis, indicating active convective heat transfer. This stage reveals how the geometry influences the spread of thermal energy and potential areas of thermal non-uniformity.

By t = 90 s (Figure 3d), the temperature field shows signs of stabilization. The gradients begin to even out, suggesting the system is approaching thermal steady-state. This uniformity is a desirable condition in drying operations, as it ensures consistent moisture removal across the entire product surface.

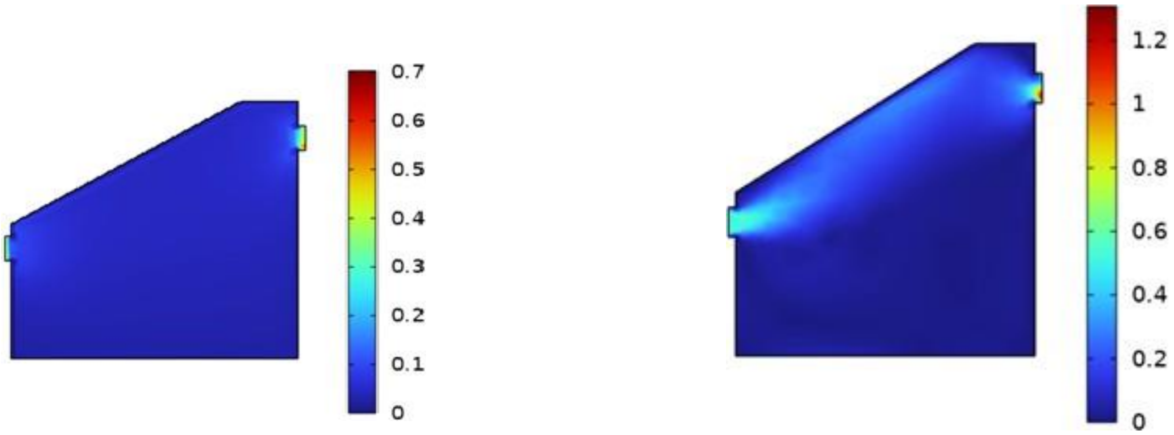

(a) Airflow at $t = 0\ s$ (b) Airflow at $t = 45\ s$

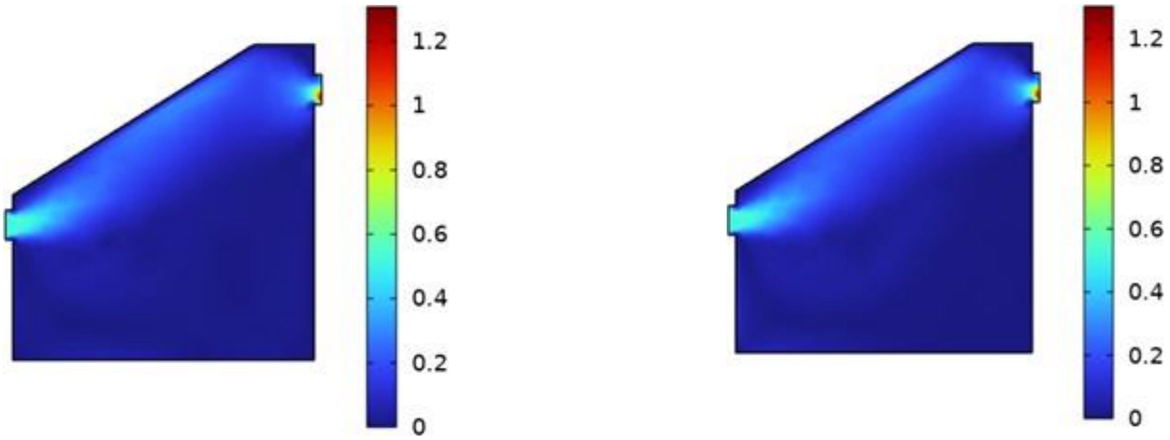

(c) Airflow at $t = 67.5\ s$ (d) Airflow at $t = 90\ s$

Figure 2: Airflow for trapezium geometric top shaped design (case 1)

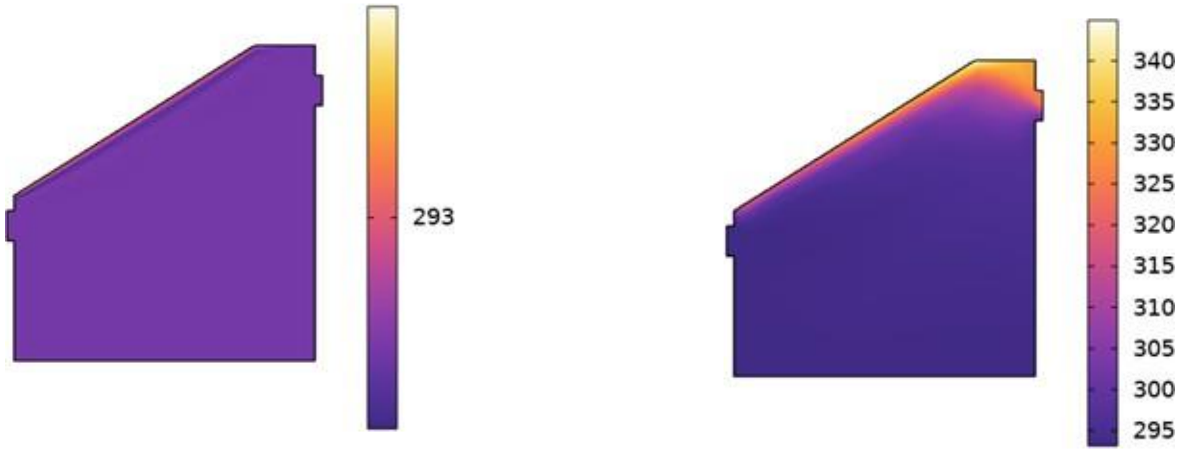

(a) Temperature at $t = 0\ s$ (b) Temperature at $t = 45\ s$

(c) Temperature at $t = 67.5\ s$ (d) Temperature at $t = 90\ s$

Figure 3: Temperature distribution for trapezium geometric top shaped design (case 1)

These findings highlight the temporal progression of heat distribution and underscore the importance of dryer geometry in facilitating efficient and uniform thermal environments for agricultural drying applications

.X TEMPORAL TEMPERATURE VARIATION AT SPECIFIC MONITORING POINTS

To further analyze the thermal performance of the solar dryer, temperature variations were monitored at two distinct spatial points: Point 1, located at the lower left-hand side, and Point 2, at the lower right-hand side of the drying chamber. These locations were chosen to

assess spatial thermal heterogeneity and the effectiveness of internal heat distribution.

Figure 4 illustrates the temporal temperature profile at Point 1. The horizontal axis represents time in seconds, ranging from 0 to 90 seconds, while the vertical axis shows temperature in Kelvin, spanning from approximately 293.14 K to 293.52 K. For the first 40 seconds, the temperature remains relatively stable around 293.16 K, indicating a thermally inert phase. This stability may be attributed to the time required to overcome the initial thermal inertia or to achieve thermal equilibrium with the surroundings.

Beyond 40 seconds, the temperature begins to rise, with a more pronounced increase observed after the 60-second mark. Between 60 and 80 seconds, the temperature elevates significantly from approximately 293.18 K to 293.52 K. This phase corresponds to an active heating regime, wherein the dryer effectively absorbs and retains solar energy, resulting in enhanced convective heating at the monitored location.

case 1. The temperature initially remains constant at around 293.15 K for the first 10 seconds, after which a gradual increase is observed. Around the 20-second mark, the temperature reaches approximately 293.25 K, followed by a brief plateau and minor fluctuations. From approximately 40 seconds onwards, a steady increase in temperature is evident, ultimately reaching around 293.6 K by the end of the observation period at 85 seconds. These observations highlight asymmetries in thermal response between the two monitored locations, which may be attributed to variations in local airflow dynamics and heat transfer characteristics within the dryer. Such spatial and temporal thermal analyses are critical for evaluating design efficiency and ensuring uniform drying conditions.

XI TEMPORAL EVOLUTION OF AIRFLOW PATTERNS FOR RECTANGULAR PRISM GEOMETRIC TOP-SHAPED DESIGN (CASE 2)

The simulation results for airflow dynamics in the solar dryer are illustrated in Figure 5 at four critical time intervals: 0, 45, 67.5, and 90 seconds. These frames provide insights into the development and stabilization of internal airflow structures over the course of the drying process.

At t = 0 seconds (Figure 5a), the airflow is largely uninfluenced by thermal gradients, ex- hibiting a uniform and undeveloped flow field. This initial state is dominated by the imposed boundary conditions and serves as a baseline for subsequent thermally driven changes.

By t = 45 seconds (Figure 5b), the onset of convective flow becomes apparent. Emerging flow patterns—such as developing streamlines and incipient vortices—indicate the initiation of thermal buoyancy effects resulting from localized heating within the chamber.

At t = 67.5 seconds (Figure 5c), the airflow becomes more structured and exhibits well-formed convective circulation. Differences in velocity magnitudes across the domain become evident, highlighting the impact of dryer geometry on internal flow guidance. This phase is critical for identifying regions with enhanced or reduced ventilation efficiency.

By t = 90 seconds (Figure 5d), the airflow reaches a quasi-steady state. The established flow field reveals distinct zones of high velocity conducive to efficient heat and moisture transfer, as well as potential stagnation areas where airflow is minimal. These spatial patterns are essential for assessing the effectiveness of the design in achieving uniform drying and minimizing energy losses.

The evolution of these airflow patterns emphasizes the importance of geometric optimization in facilitating uniform convective flow and improving the overall performance of the solar dryer.

XII AIRFLOW SIMULATION RESULTS FOR THE TRIANGULAR PRISM DRYER DESIGN

The airflow simulation results for the third geometric configuration of the solar dryer are analyzed at four distinct time intervals: t = 0 s, t = 45 s, t = 67.5 s, and t = 90 s- (Figure 6). These snapshots capture the temporal evolution of airflow dynamics within the drying chamber and reveal the influence of structural design on convective flow behavior.

At the initial time step t = 0 s (Figure 6(a)), the airflow field is characterized by a uniform and undeveloped velocity distribution. This suggests a stable initialization of the simulation with no significant internal re-circulation or buoyancy effects present. The airflow remains largely unstructured, serving as the baseline condition prior to any thermally induced motion.

By t = 45 s (Figure 6(b)), the airflow begins to exhibit more pronounced spatial variations. The emergence of streamlines and localized vertical structures indicates the onset of thermally driven convection, induced by solar heating of the internal surfaces. These patterns reflect the influence of the dryer's geometry in shaping internal airflow paths.

At t = 67.5 s (Figure 6(c)), the airflow develops into a more complex and coherent structure. Convective cells and turbulent eddies become increasingly visible, suggesting enhanced air mixing and distribution within the chamber. This phase is particularly important for evaluating zones of high and low air velocity as these directly affect drying uniformity and moisture removal efficiency.

By the final observation at t = 90 s (Figure 6(d)), the flow field reaches a quasi-steady state. The airflow patterns stabilize, highlighting regions of sustained high velocity conducive to effective drying, as well as potential stagnation zones where airflow is limited These results are critical for assessing the long-term performance of the dryer and for identifying areas where geometric improvements could further optimize airflow distribution.

Overall, the temporal analysis underscores the importance of dryer design in promoting efficient and uniform airflow, which is essential for enhancing drying performance and minimizing energy losses.

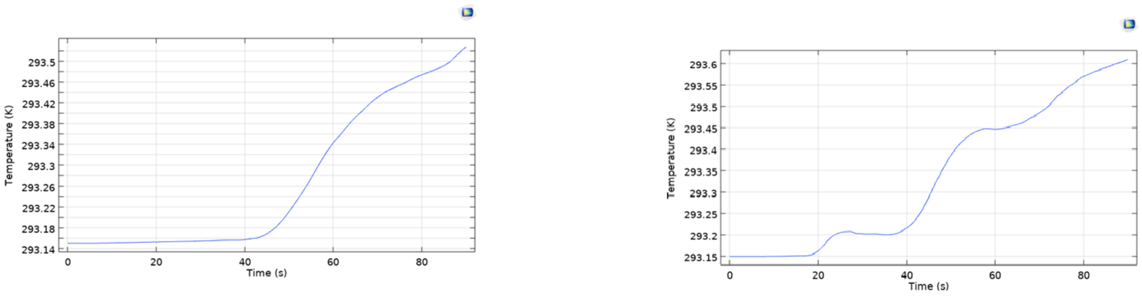

(a) Temperature at t = 0 s

(b) Temperature at t = 45 s

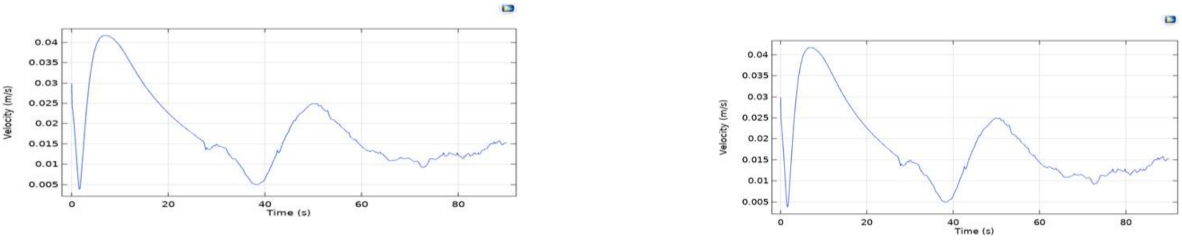

(c) Temperature at t = 67.5s

(d) Temperature at t = 90 s

Figure 4: Graph showing velocity variation at point 2 in case 1

(a) Airflow at *t* = 0 *s*

(b) Airflow at *t* = 45 *s*

(c) Airflow at t = 67.5 s

(d) Airflow at t = 90 s

Figure 5: Temperature distribution for rectangular prism geometric top shaped design (case 2)

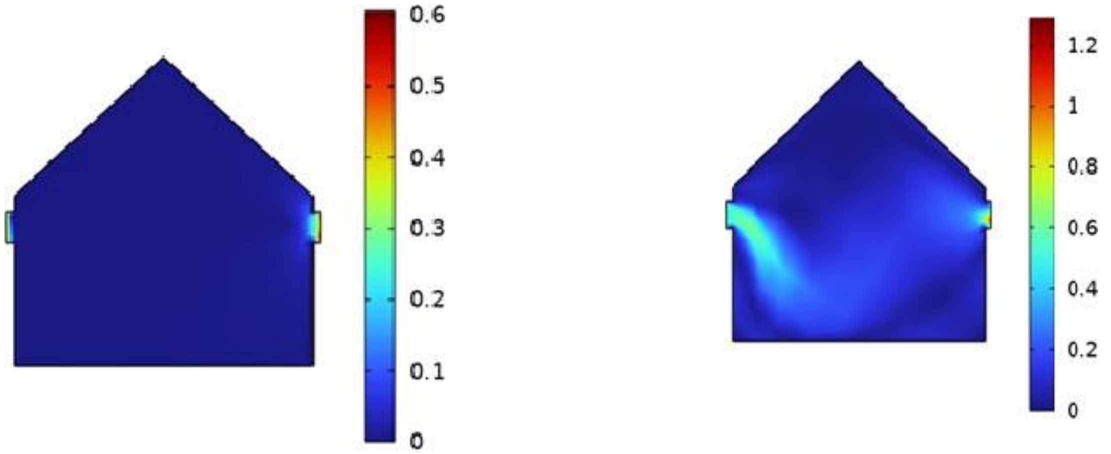

(a) Airflow at t = 0 s

(b) Airflow at t = 45 s

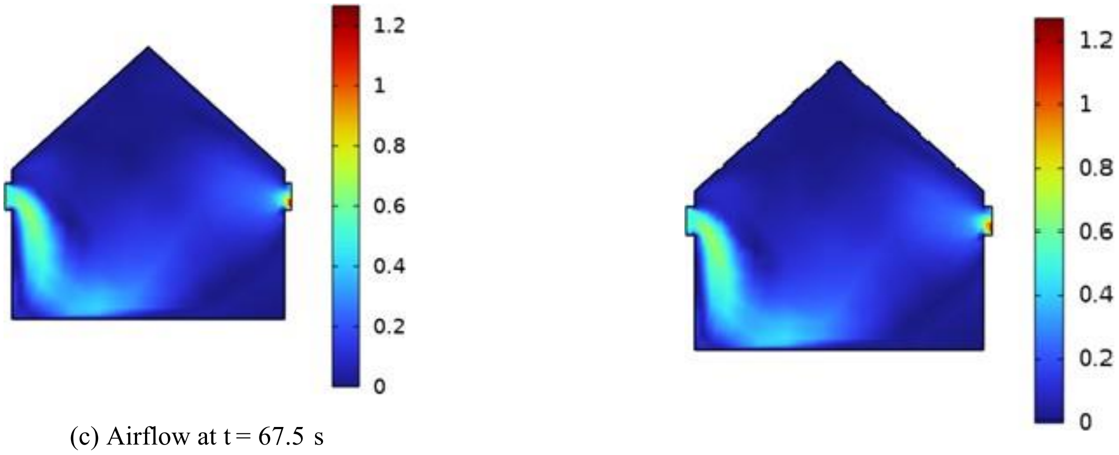

(c) Airflow at t = 67.5 s

(d) Airflow at t = 90 s

Figure 6: Airflow for triangular prism geometric top shaped design (case 3)

XIII DISCUSSION

The simulation results provide critical insights into the transient behavior of airflow and temperature distribution within the three solar dryer designs. Across all geometries, airflow evolved from an initially uniform state to complex, structured patterns influenced by internal geometry and buoyancy-driven convection. The triangular prism design consistently demonstrated more uniform airflow and minimized stagnation zones, which are key for enhancing convective heat transfer and avoiding localized moisture retention.

Temporal temperature profiles revealed that internal heating was gradual, with notable tem- perature rise commencing around 40–60 seconds into the simulation. Point-based temperature monitoring at both left and right lower ends of the chamber confirmed thermal asymmetries and highlighted the importance of structural orientation in achieving uniform thermal distribution. The triangular dryer achieved the most balanced temperature field at t = 90 s, indicating superior thermal performance.

The evolution of flow patterns from undeveloped fields to quasi-steady circulations confirms the role of dryer geometry in modulating internal dynamics. Streamlines and vertices were most coherent and evenly distributed in the triangular configuration, suggesting efficient air exchange and reduced dead zones.

Overall, the study confirms that geometric optimization significantly influences dryer efficiency. The triangular prism design outperforms the rectangular and trapezoidal geometries in both airflow and temperature uniformity, making it a promising candidate for field deployment in agricultural drying systems.

XI V CONCLUSION

In summary, while traditional drying methods continue to play a significant role in agricultural practices, they often need to be improved for modern food production's demands, particularly in regions where food security is a critical concern. Solar drying technologies offer a viable alternative, providing a cleaner, more efficient, and environmentally sustainable solution for preserving agricultural produce. However, to fully harness the potential of these technologies, it is essential to optimize their design and operation using advanced tools such as Compu- tational Fluid Dynamics. Doing so can significantly reduce post-harvest losses, improve the quality of dried agricultural products, and support the broader goals of sustainable agriculture and food security

LIST OF ABREVIATIONS

CFD: Computational Fluid Dynamics, GDP: Gross Domestic Product

FUNDING

Not Applicable

CONSENT OF PUBLICATION

Npt applicable

COMPETING INTERESTS

Authors have no competing interest.

REFERENCES

[1] Food and Agriculture Organization, The State of Food and Agriculture 2021: Making agrifood systems more resilient to shocks and stresses,

[2] Pawlak, Karolina and Ko lodziejczak, Ma lgorzata. The role of agriculture in ensuring food security in developing countries: Considerations in the context of the problem of sustainable food production, MDPI, 12(13), pp. 5488

[3] M, Taddesse. Post-harvest loss of stored grain, its causes and reduction strategies, Food Science and Quality Management, 2020, vol. 96, pp. 26–35.

[4] Tiwari and Anupam. A review on solar drying of agricultural produce, Journal of Food Processing and Technology, 2016, vol. 7, pp. 1–12.

[5] E. Crist, and C. Mora, and R. Engelman. The interaction of human population, food production, and biodiversity protection, *rican* Association for the Advancement of Science, vol. 356 , pp. 260–264

[6] H. Affognon, and C. Mutungi, and P. Sanginga, and C. Borgemeister. Unpacking postharvest losses in sub-Sahara Africa: A meta-analysis, World Development, 2015, vol. 66, pp. 49–68

[7] Sahdev, K. Ravinde. Open sun and greenhouse drying of agricultural and food products: a review, International Journal of Engineering Research.2014, Vol 3

[8] V. Belessiotis, and E. Delyannis. Solar drying: An overview of recent develop- ments. Energy Conversion and Management. 2011, Vol. 52, pp. 1190–1201.

[9] A. Esper, and W. Mühlbauer. Solar drying An effective means of food preservation. Renewable Energy ,1998.

.

[10] A. Sharma, and C. R. Chen, and N.V Lan, Solar-energy drying systems: A review, Renewable and Sustainable Energy Reviews. 2009, Vol. 13, pp. 1185–1210

[11] S. Janjai. A greenhouse type solar dryer for small-scale dried food industries: Development and dissemination. International Journal of Energy and Environment. 2012, pp. 383–398

[12] A. Kumar, and G.N Tiwari, and S. Sinha. Design, construction and performance evaluation of a solar crop dryer for rural applications. Energy Conversion and Management 2016, vol. 47, pp. 2941–2949.

[13] R.K . Goyal, and G.N. Tiwari, Parametric study of a reverse flat plate absorber cabinet dryer: A new concept. Solar Energy. 2007, vol. 81, pp. 853–861.